Supporting Information to Accompany:

Ruthenium–Thymine Acetate binding modes: Experimental and Theoretical Studies

Silvia Bordoni*†, Stefano Cerini†, Riccardo Tarroni†, Magda Monari‡, Carla Boga†

†Dipartimento di Chimica Industriale "Toso Montanari", Università di Bologna, Viale Risorgimento 4, I-40136 Bologna, Italy

‡Dipartimento di Chimica "Giacomo Ciamician", Università di Bologna, Via Selmi 2, I-40126 Bologna, Italy

Table of Contents

Table S1. Crystal data and structure refinement for compound ***cis*-2**

Compound	*cis*-**2**
Formula	$C_{51}H_{44}N_4O_9P_2Ru$
Fw	1019.91
T, K	296
λ, Å	0.71073
Crystal symmetry	Monoclinic
Space group	$P2_1/n$
a, Å	14.895(3)
b, Å	13.501(3)
c, Å	25.513(5)
α	90
β	100.836(2)
γ	90
Cell volume, $Å^3$	5039.4(18)
Z	4
D_c, Mg m^{-3}	1.344
μ(Mo-Kα), mm^{-1}	0.432
F(000)	2096
Crystal size/ mm	0.25 x 0.20 x 0.15
θ limits, °	1.474 - 25.013
Reflections collected	44083
Unique obs. Reflections [$F_o > 4\sigma(F_o)$]	8809 [R(int) = 0.1153
Goodness-of-fit-on F^2	0.939
R_1 $(F)^a$, wR_2 (F^2) [$I > 2\sigma(I)$]	0.0706, 0.1068
Largest diff. peak and hole, e. $Å^{-3}$	0.455 and -0.378

[a] $R_1 = \Sigma||F_o|-|F_c||/\Sigma|F_o|$.[b] $wR_2 = [\Sigma w(F_o^2-F_c^2)^2/\Sigma w(F_o^2)^2]^{1/2}$ where $w = 1/[\sigma^2(F_o^2) + (aP)^2 + bP]$ where $P = (F_o^2 + F_c^2)/3$.

Table S2. Most relevant hydrogen bonds for ***cis*-2** [Å and °].

D-H...A	d(D-H)	d(H...A)	d(D...A)	<(DHA)
N(2)-H(2N)···O(7)#1	0.86	2.12	2.798(9)	134.8
N(4)-H(4N)···O(4)#1	0.86	2.05	2.893(10)	164.8

Symmetry transformations used to generate equivalent atoms:

#1 -x+3/2,y-1/2,-z+1/2 #2 -x+1,-y+1,-z

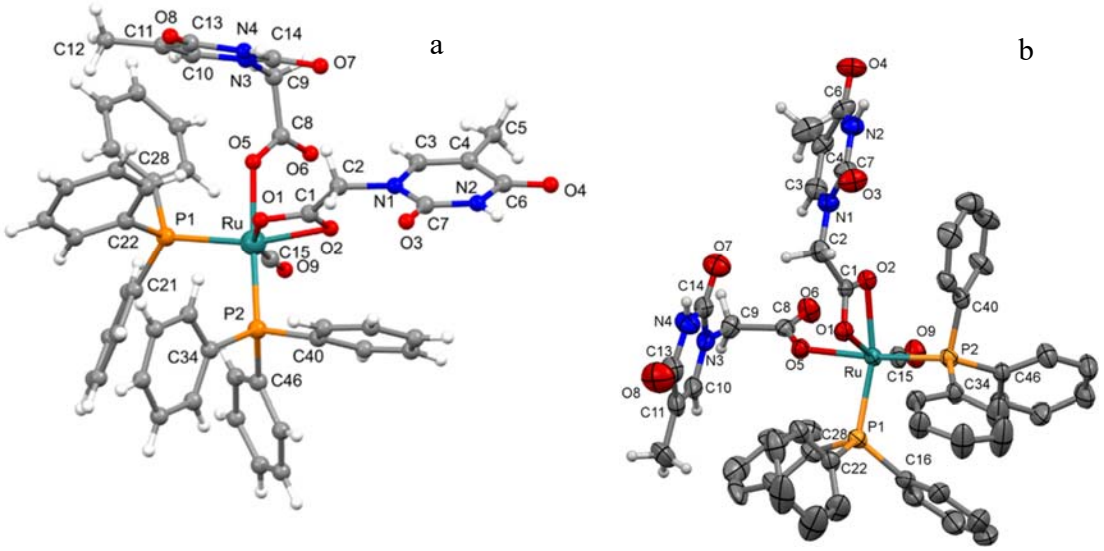

Figure S1. a) Molecular structure of ***cis*-2** with the atom labelling, b) ORTEP drawing of ***cis*-2** (thermal ellipsoids are drawn at the 30% of the probability level) with the atom labelling scheme. The phenyl H atoms have been omitted for the sake of clarity.

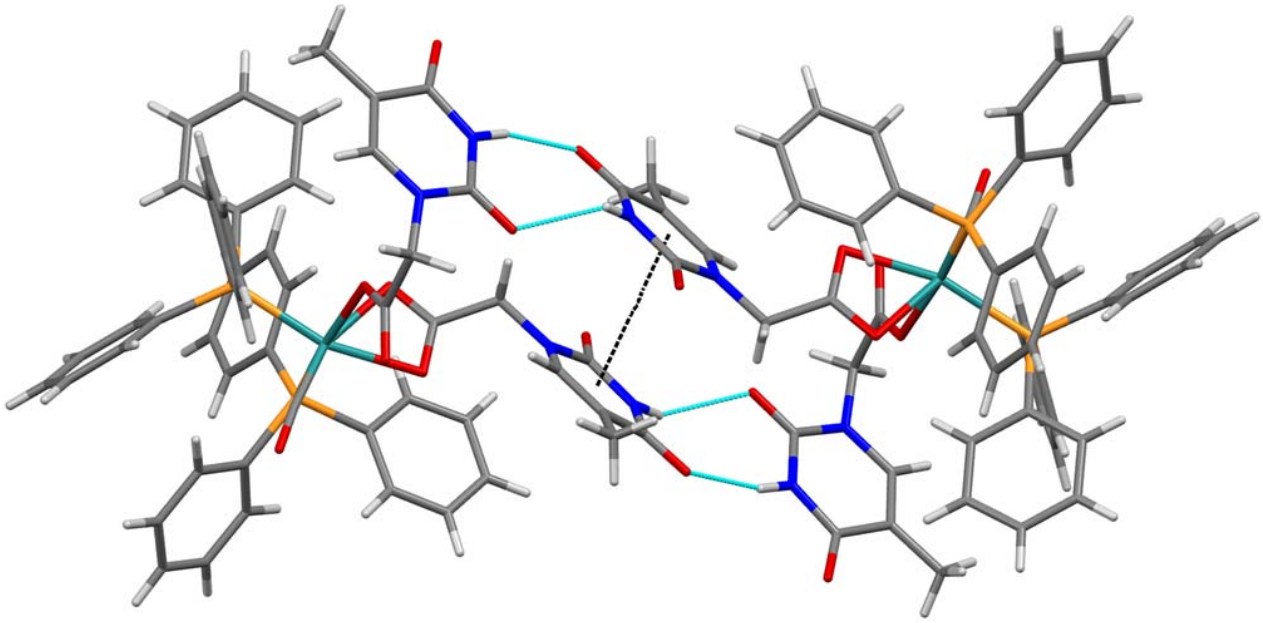

Figure S2. Molecular structure of ***cis*-2** with π-π stacking and Watson-Crick intermolecular interaction

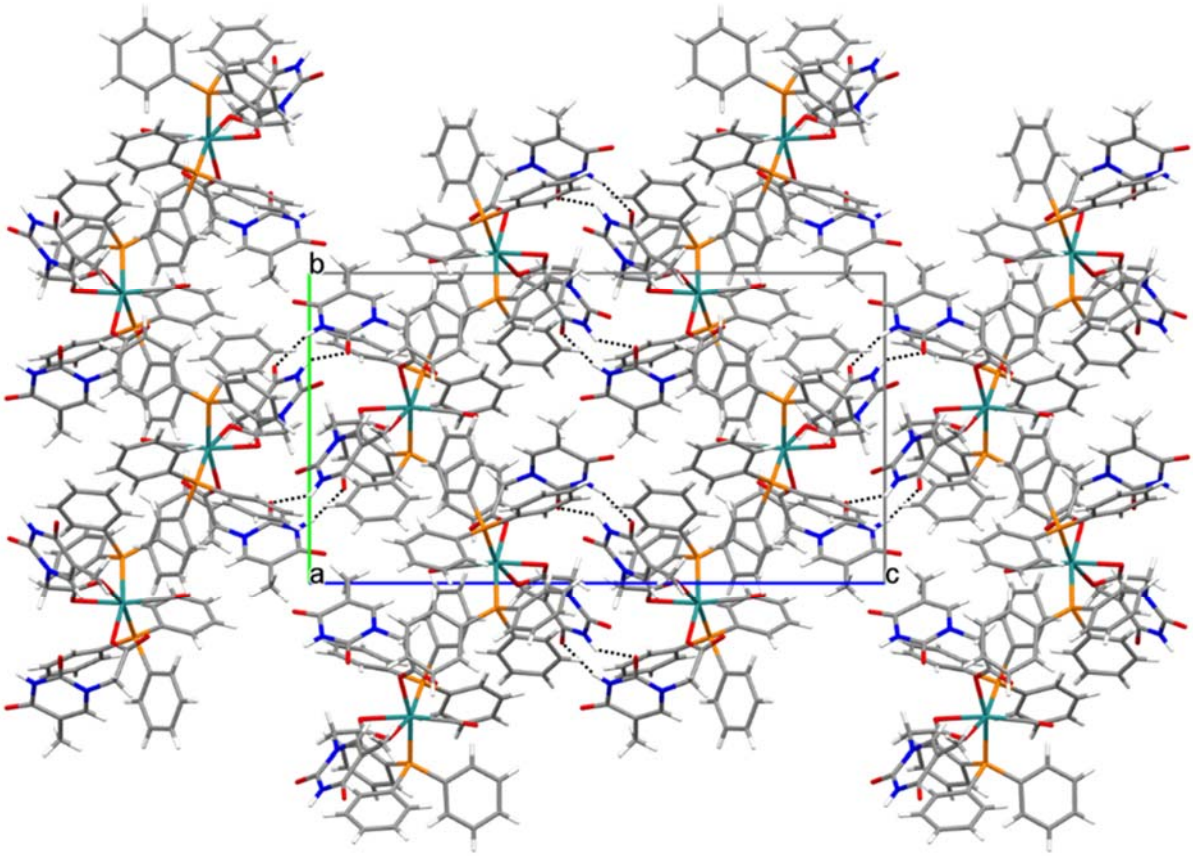

Figure S3. View down. Fragment of the crystal packing of complex **2** illustrating the intermolecular H bonding pattern. For the sake of clarity only the H atoms engaged in H bonds are shown. Ball and stick representation is used for the dimer arising by the strong N-H···O hydrogen bonding and for the atoms connected to it. H bonds are shown with blue dashed lines. The *a* axis of the crystal packing of ***cis*-2**. Black dotted lines indicate the intermolecular N-H···O hydrogen bonds.

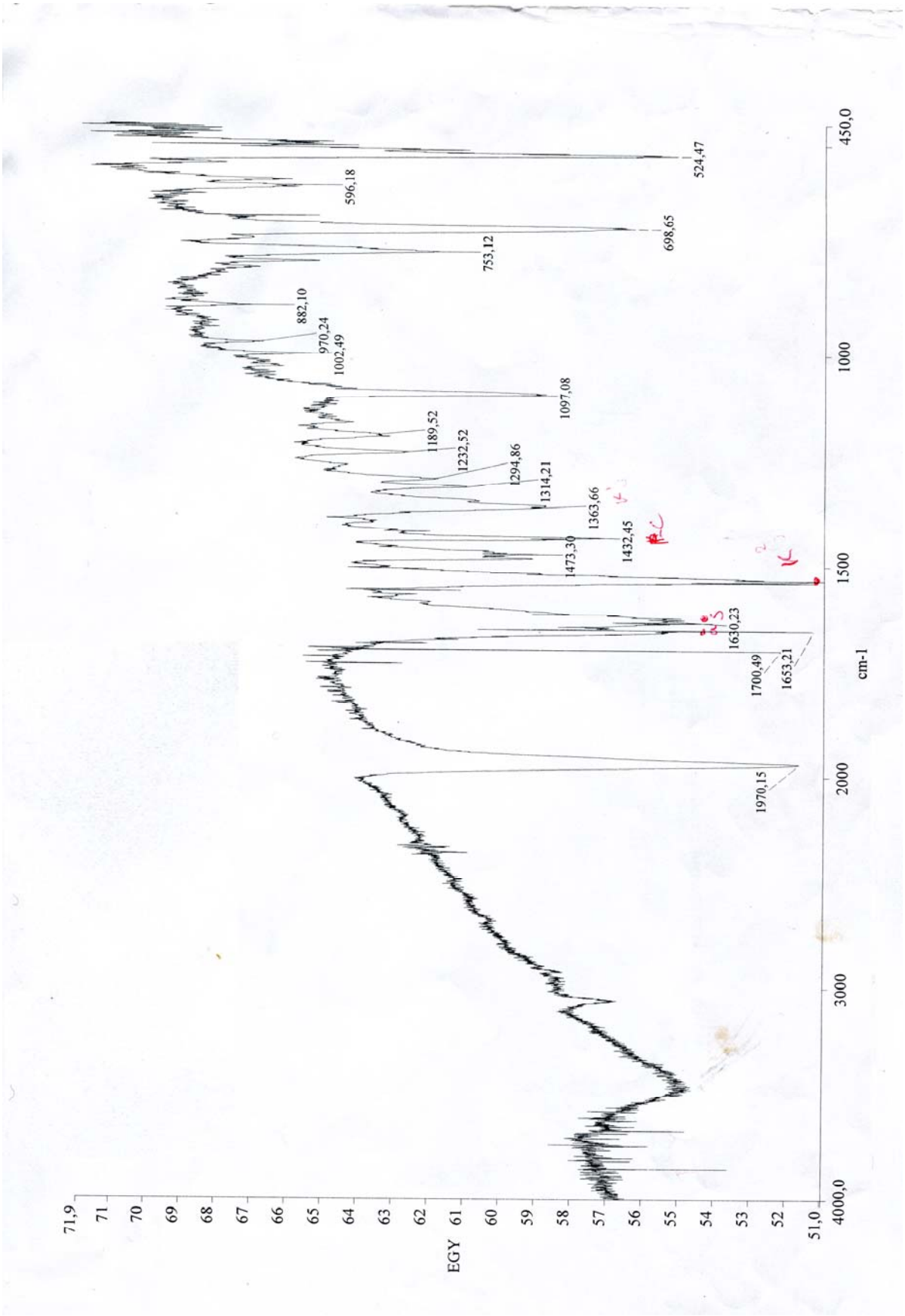

Figure S4. FTIR of of *trans*-{Ru(CO)(PPh_3)$_2$[κ^1(O)THAc][κ^2(O,O)THAc]} **2**

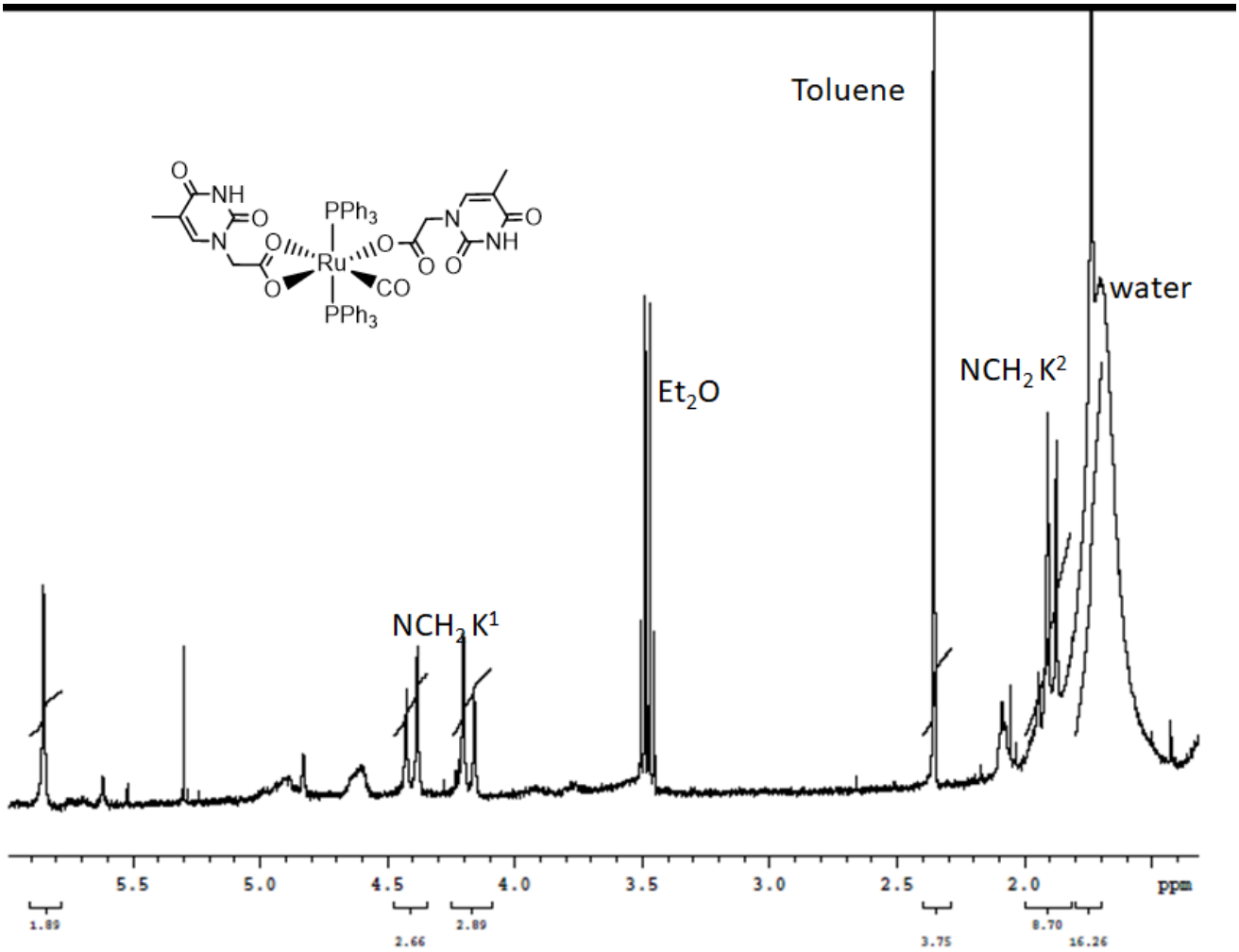

Figure S5a. ^{1}H-NMR (400 MHz) of *trans*-{Ru(CO)(PPh$_3$)$_2$[κ^1(O)THAc][κ^2(O,O)THAc]} **2** in CDCl$_3$

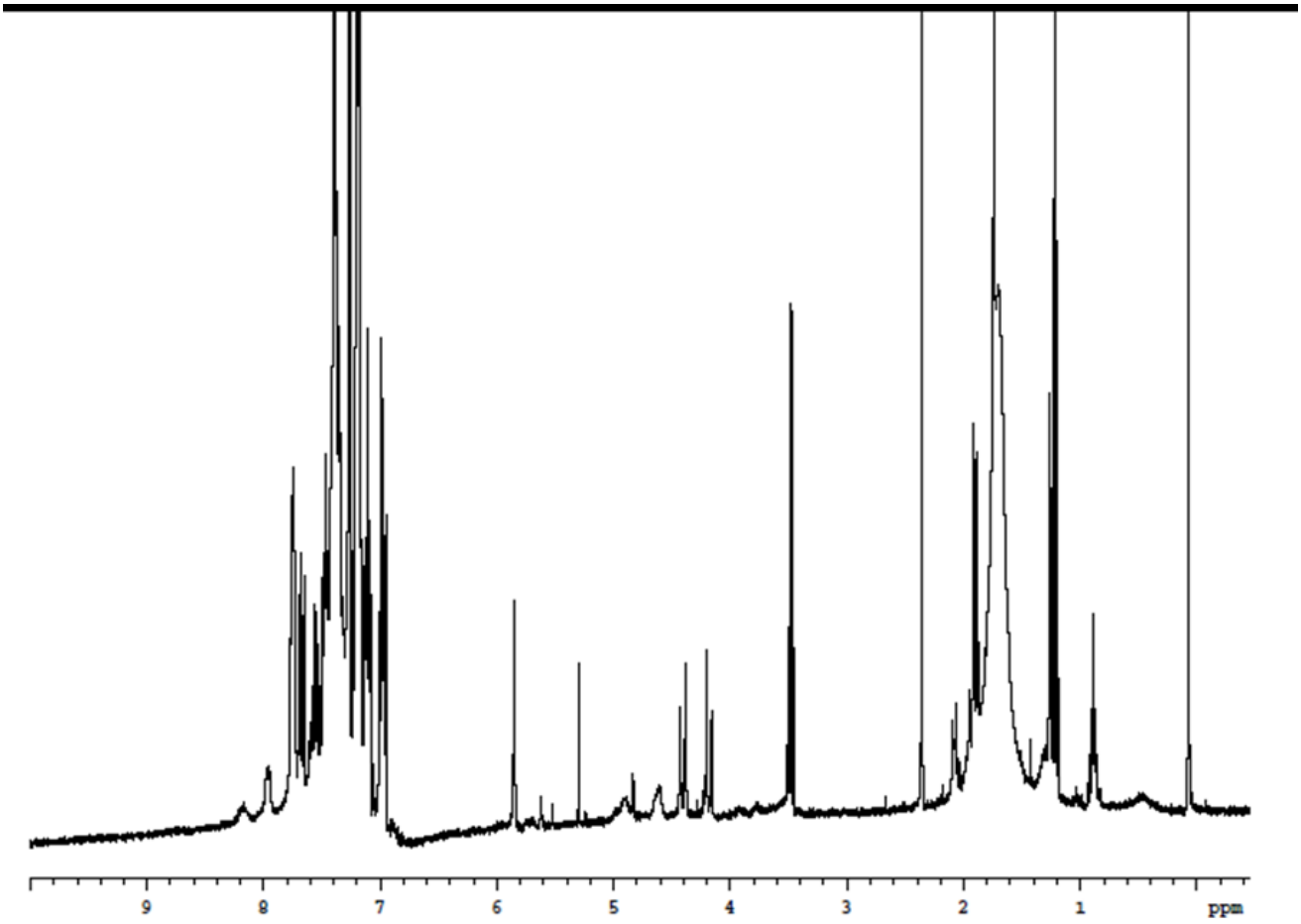

Figure S5b. ^{1}H-NMR (400 MHz) of *trans*-{Ru(CO)(PPh_3)$_2$[κ^1(O)THAc][κ^2(O,O)THAc]} **2** in $CDCl_3$

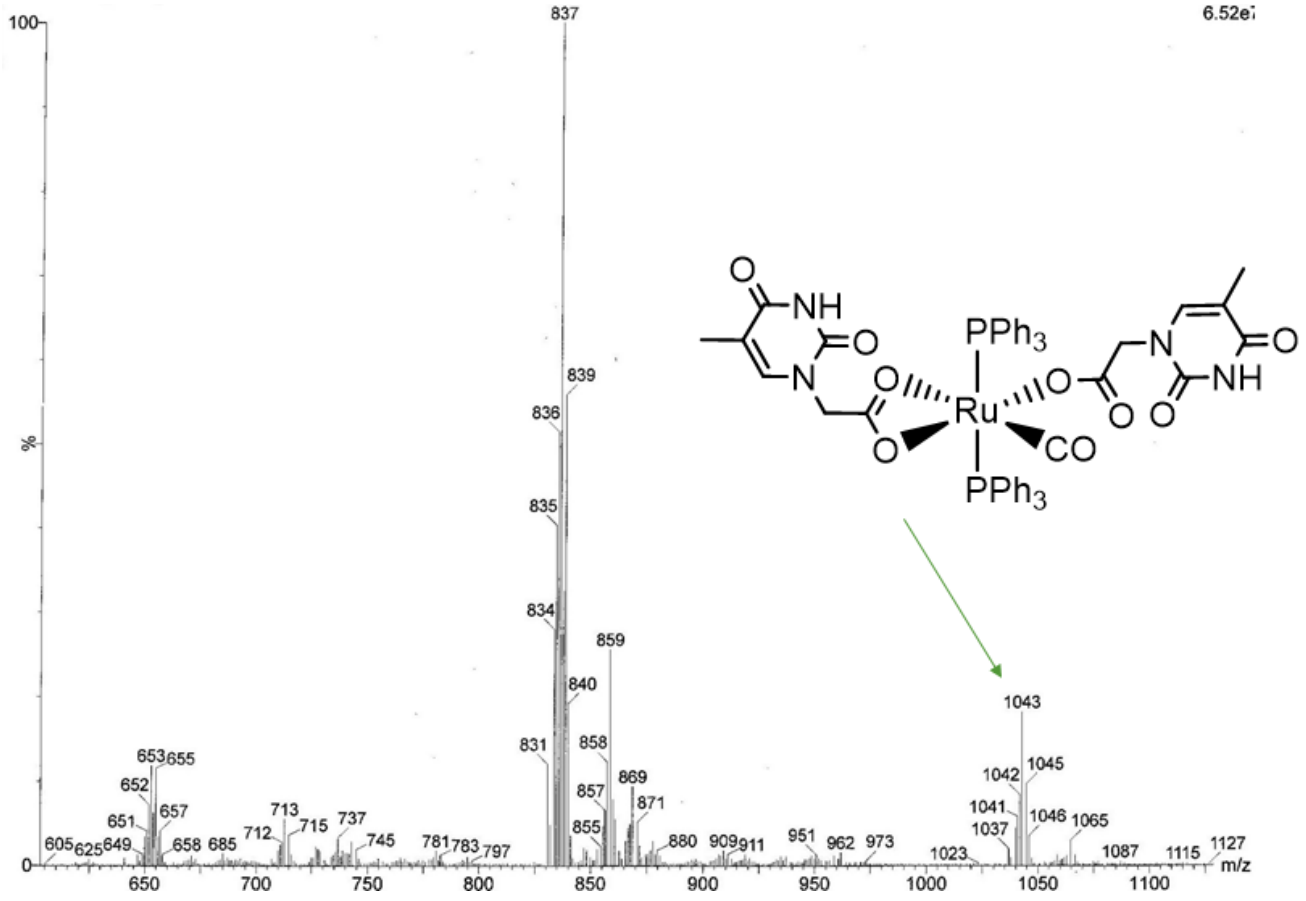

Figure S6. ESI-MS of of *cis*-{Ru(CO)(PPh_3)$_2$[κ^1(O)THAc][κ^2(O,O)THAc]} **2**

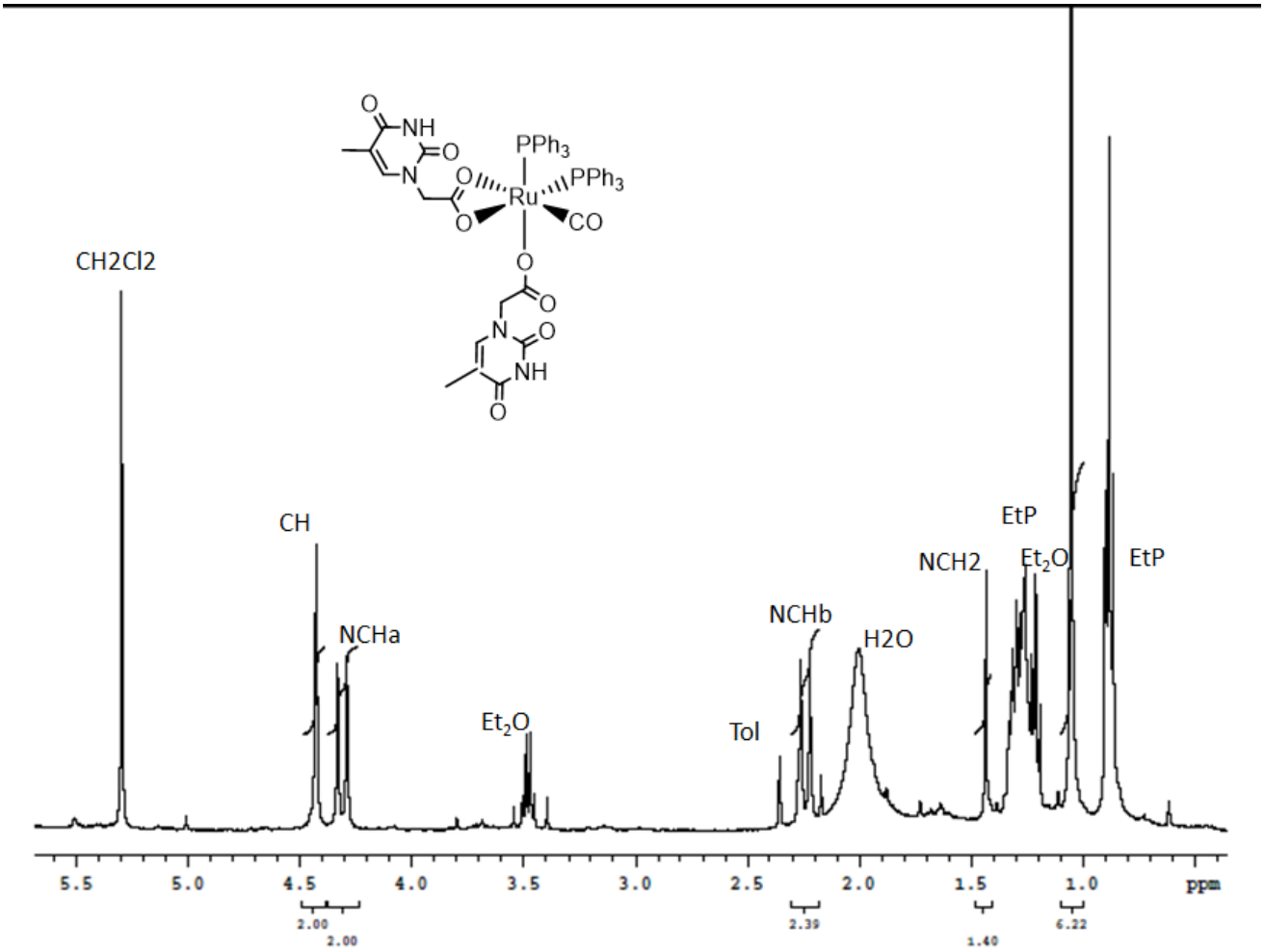

Figure S7a. ^{1}H-NMR (400 MHz) of *cis*-{Ru(CO)(PPh_3)$_2$[κ^1(O)THAc][κ^2(O,O)THAc]} **2** in $CDCl_3$

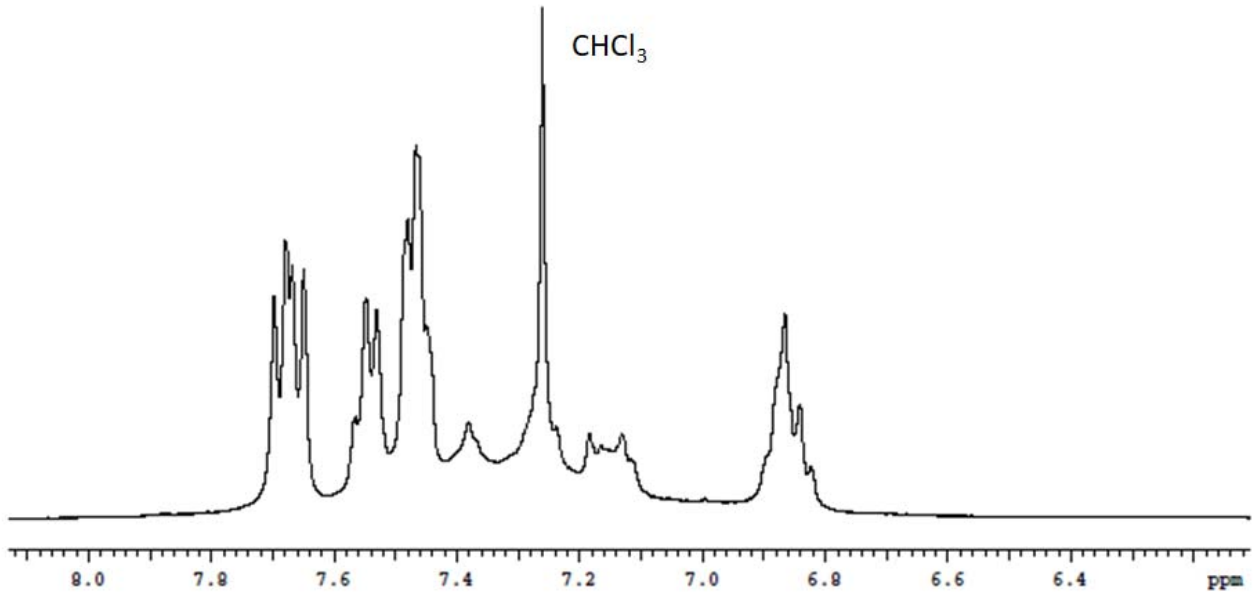

Figure S7b. ^{1}H-NMR (400 MHz) of *cis*-{Ru(CO)(PPh_3)$_2$[κ^1(O)THAc][κ^2(O,O)THAc]} **2** aromatic region in $CDCl_3$

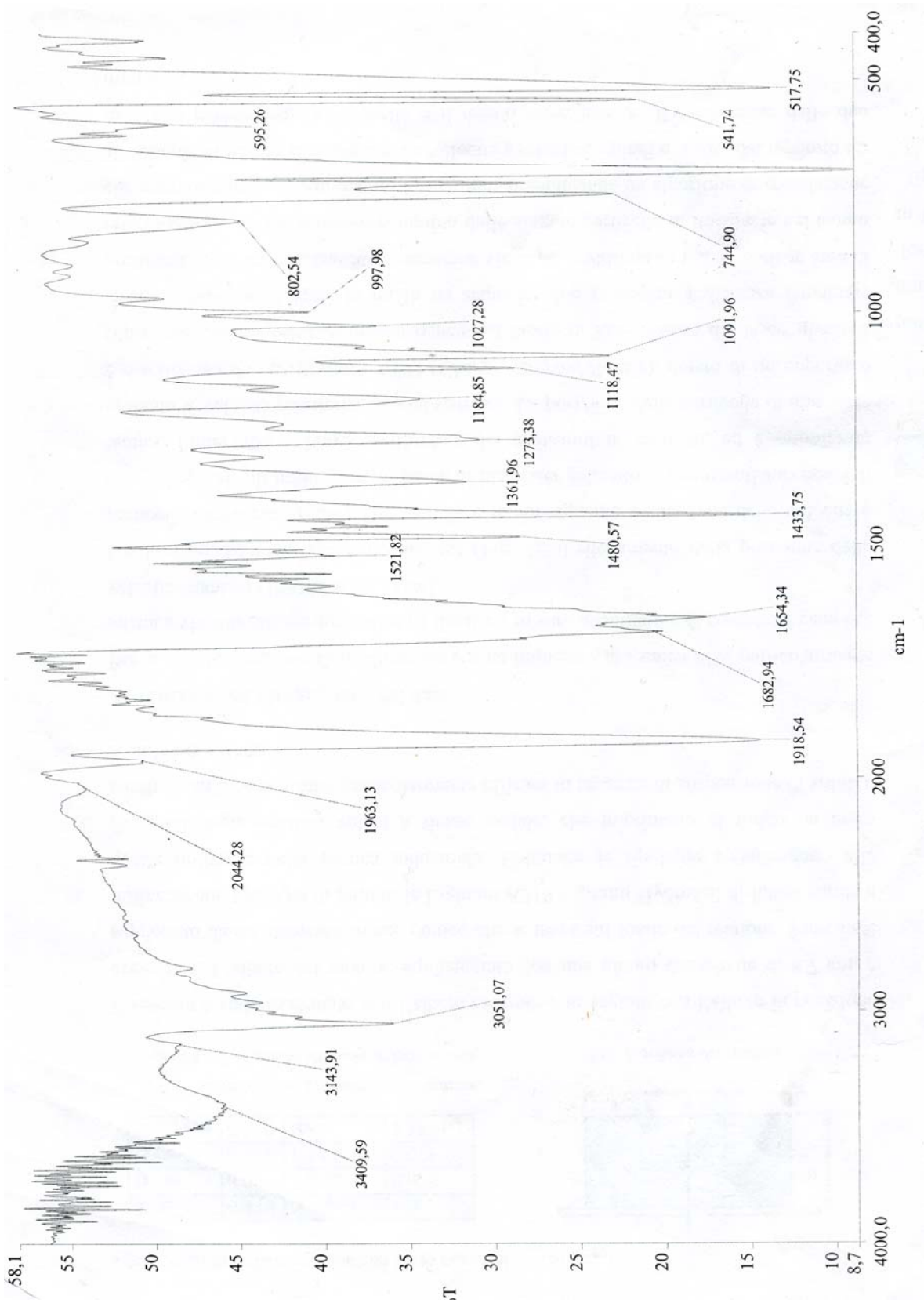

Figure S8. FTIR spectrum of **3 a,b**

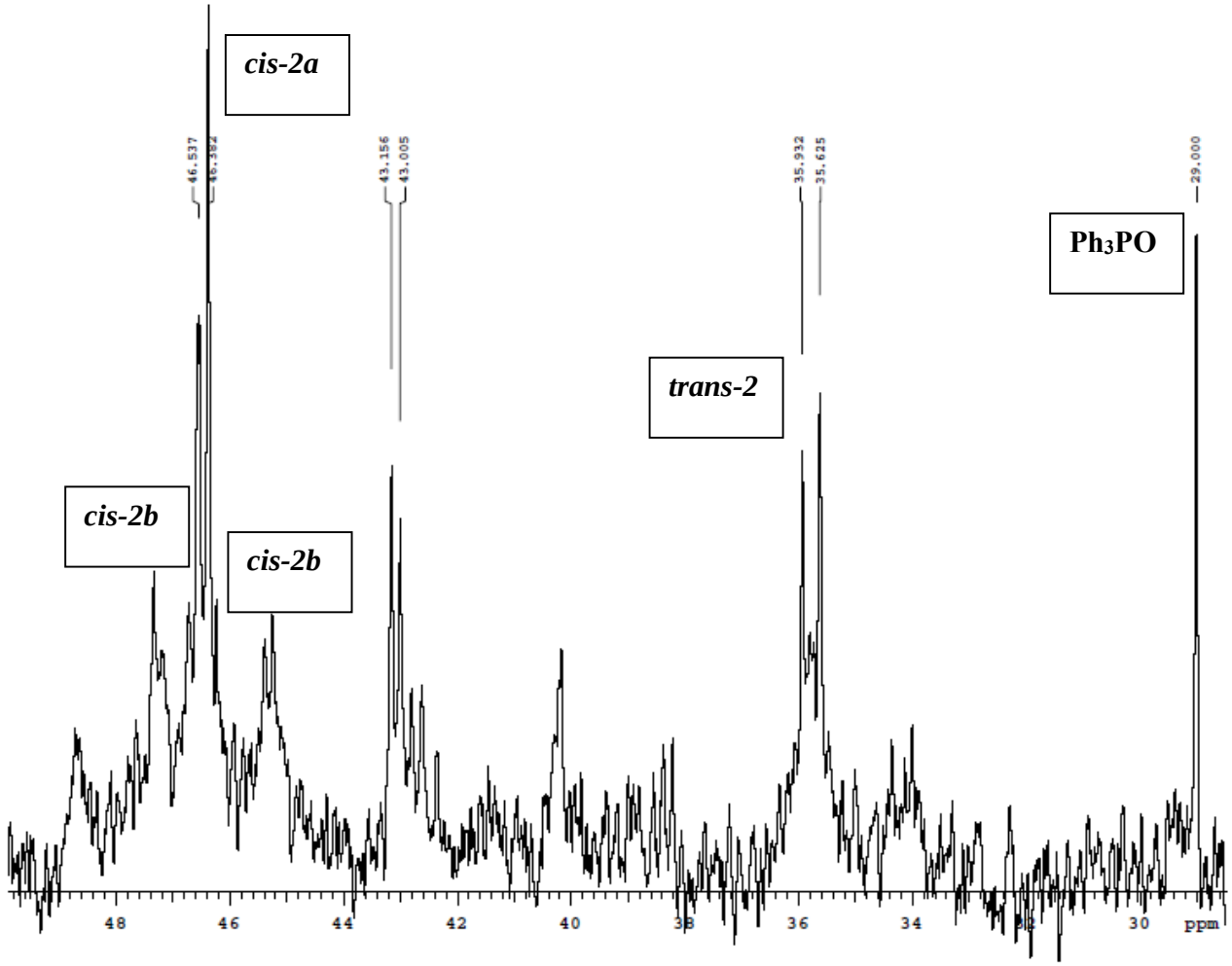

Figure S9. ^{31}P-NMR (161 MHz) of **2** in $CDCl_3$

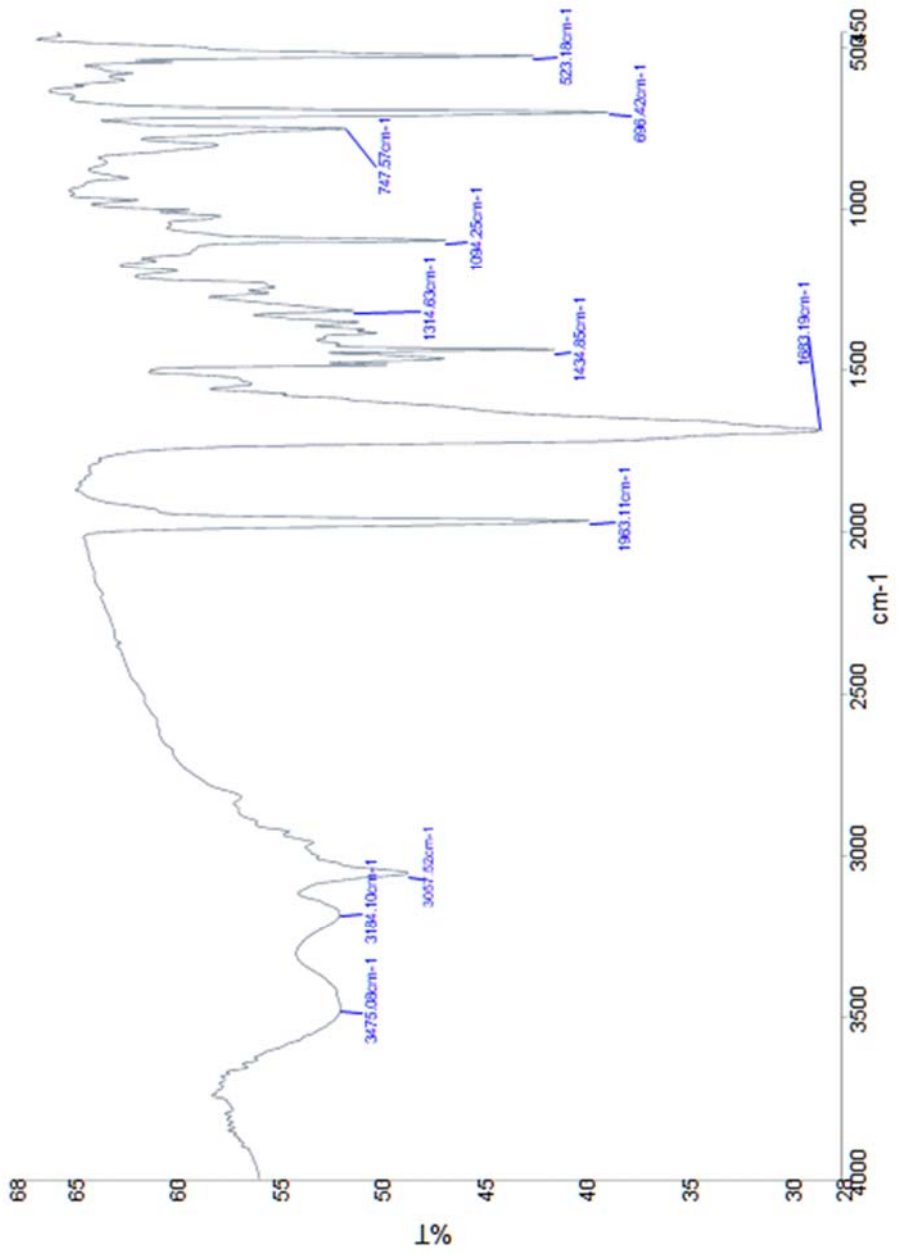

Figure S10. FT-IR (KBr) k^2(O,O)-RuH(CO)(THAc)(PPh_3)$_2$ **4**

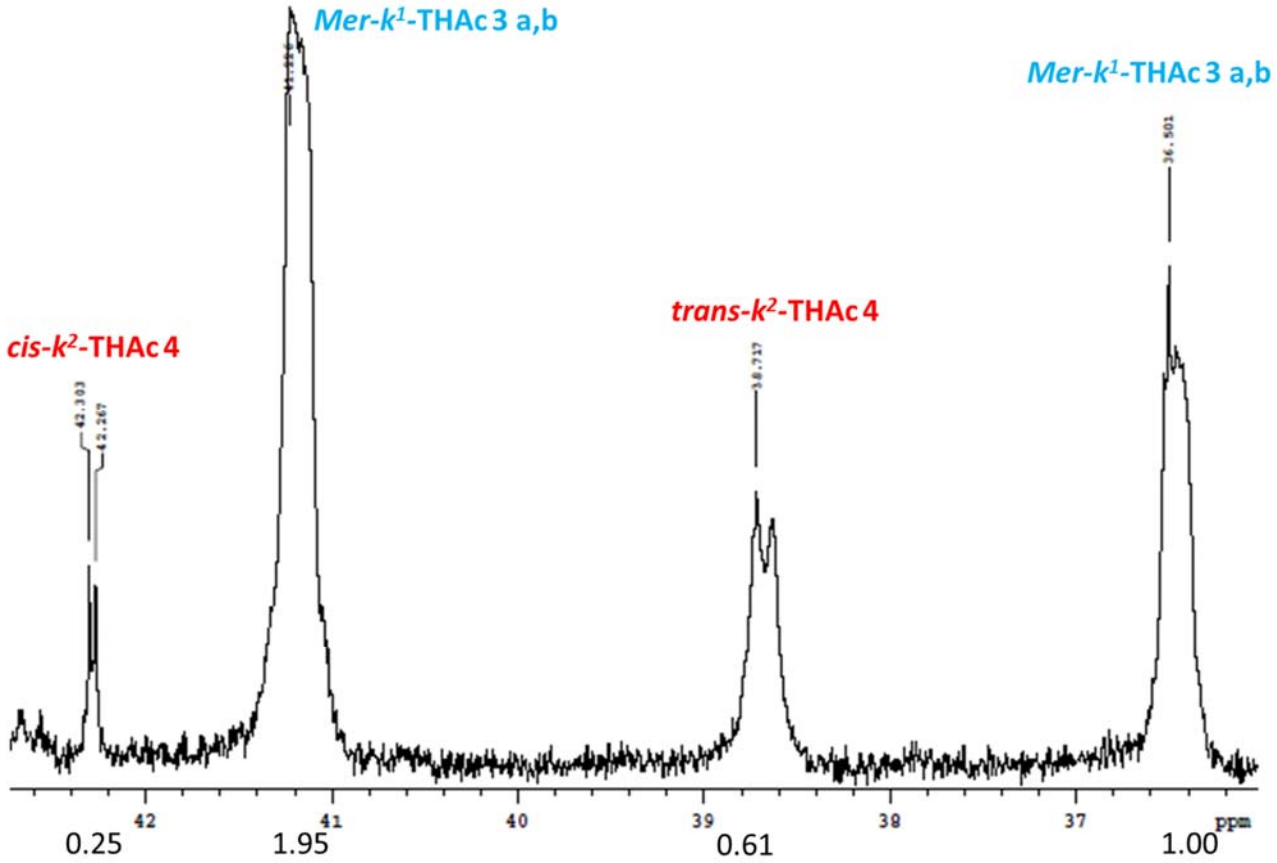

Figure S11a. $^{31}P\{^{1}H\}$-NMR (161,9 MHz) $k^1(O)$-[RuH(CO)(THAc)$(PPh_3)_3$ **3** + $k^2(O,O)$-RuH(CO)(THAc)$(PPh_3)_2$ **4** in (**3**:**4**=3:0,8) $CDCl_3$

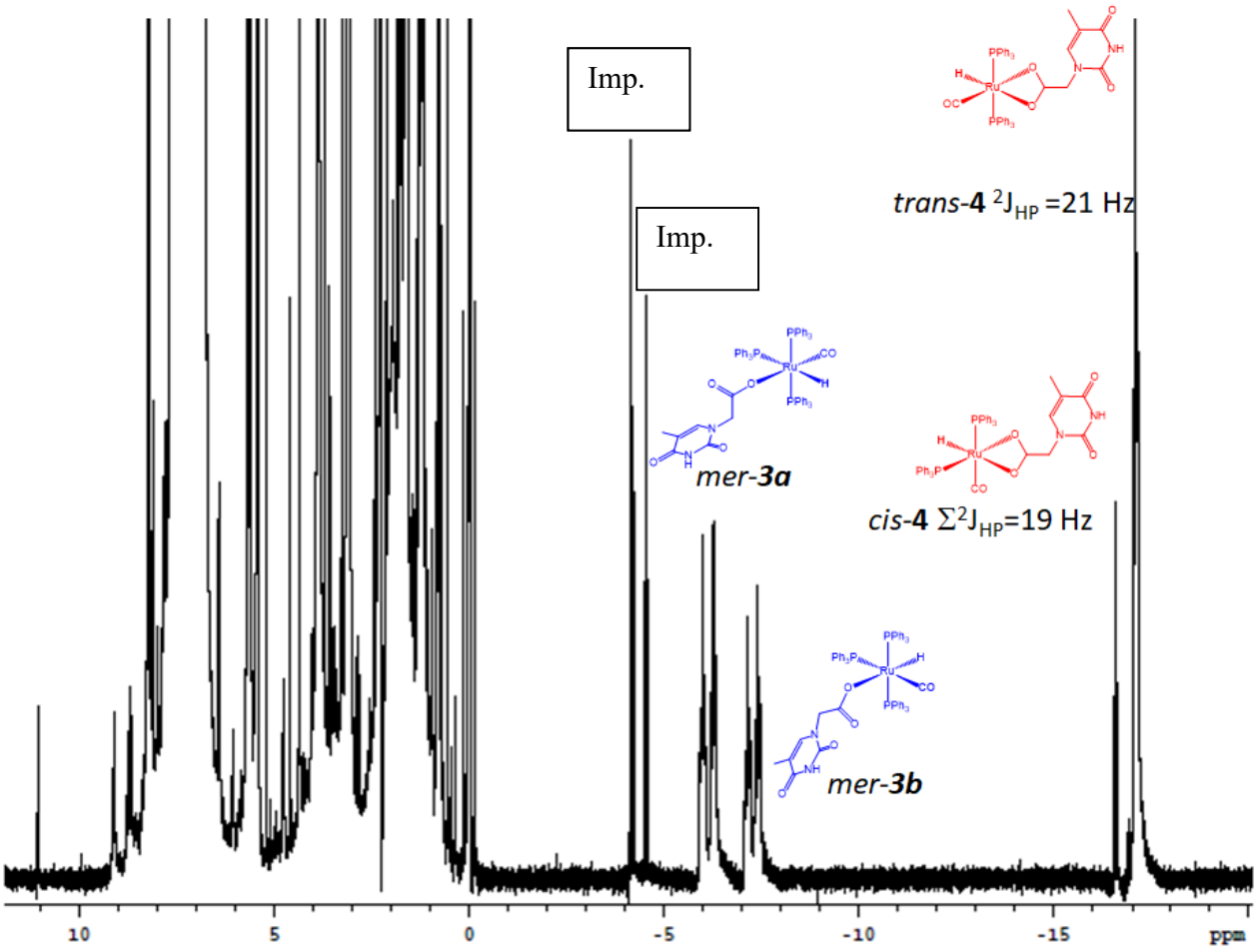

Figure S11b. ^{1}H-NMR spectrum of **3** +**4** (ratio 3:2) in $CDCl_3$

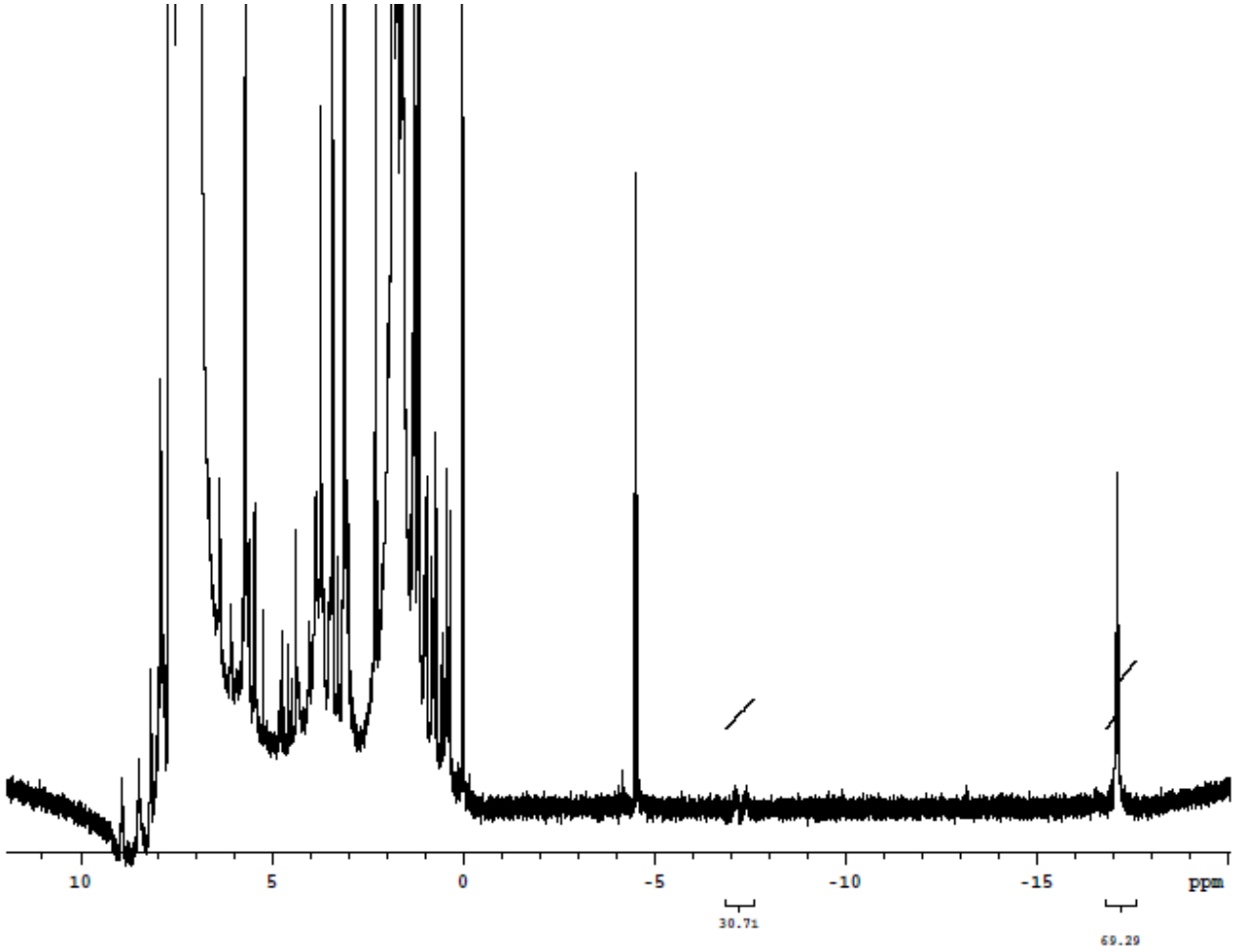

Figure S11c. ^{1}H-NMR spectrum of **3** +**4** (ratio 3:7) in $CDCl_3$

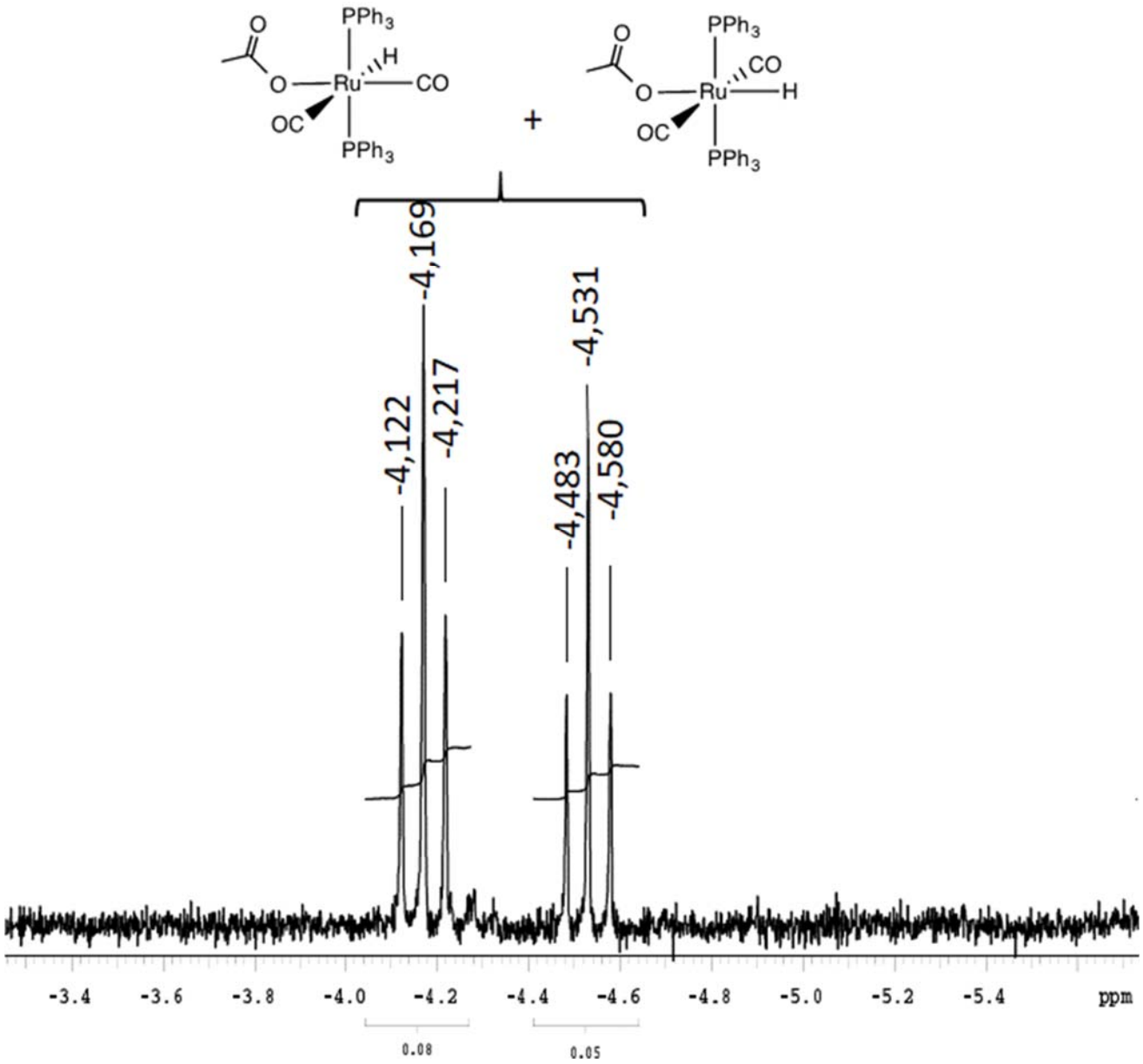

Figure 11d. Complexes formed as impurities during the preparative reduction of starting material **1**

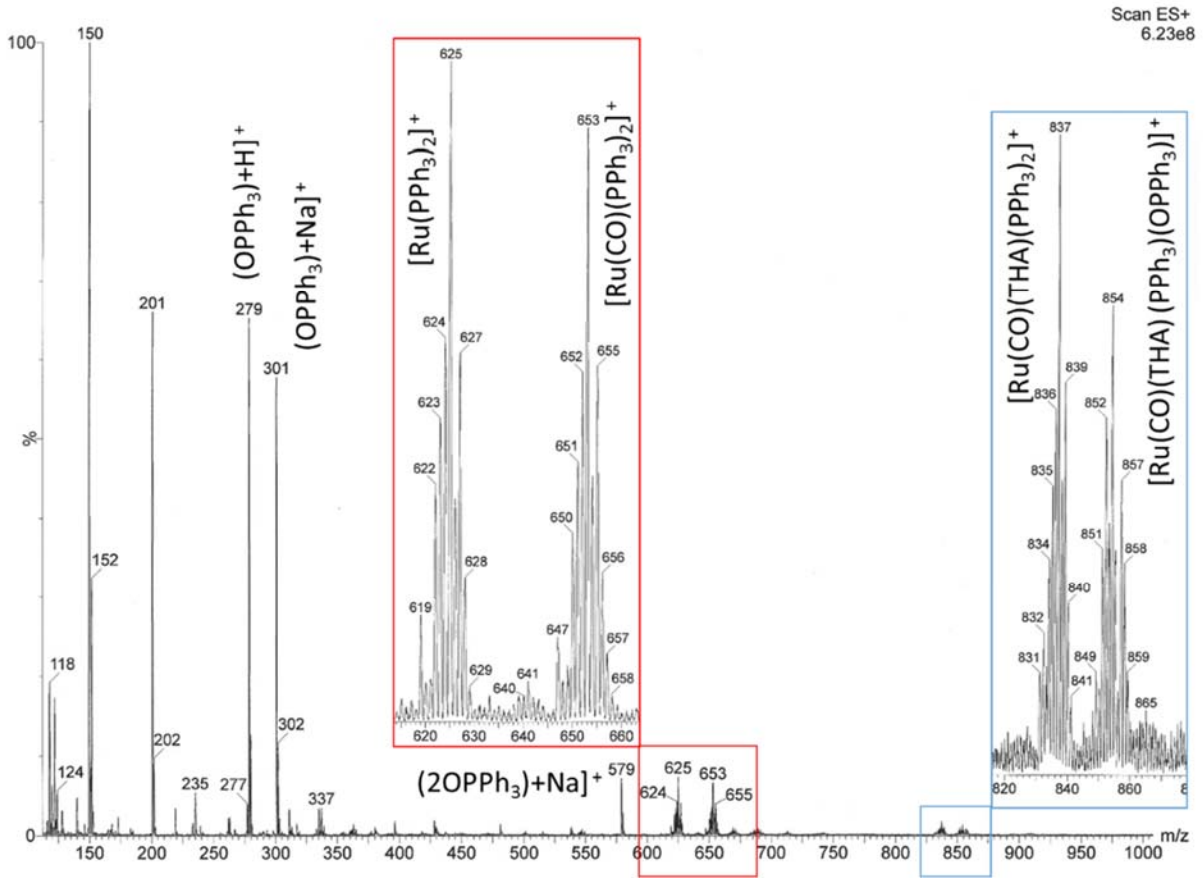

Figure S12. ESI-MS (MeOH) of κ^2(O,O){HRu(CO)(PPh_3)$_2$[κ^2(O,O)THAc]} **4**

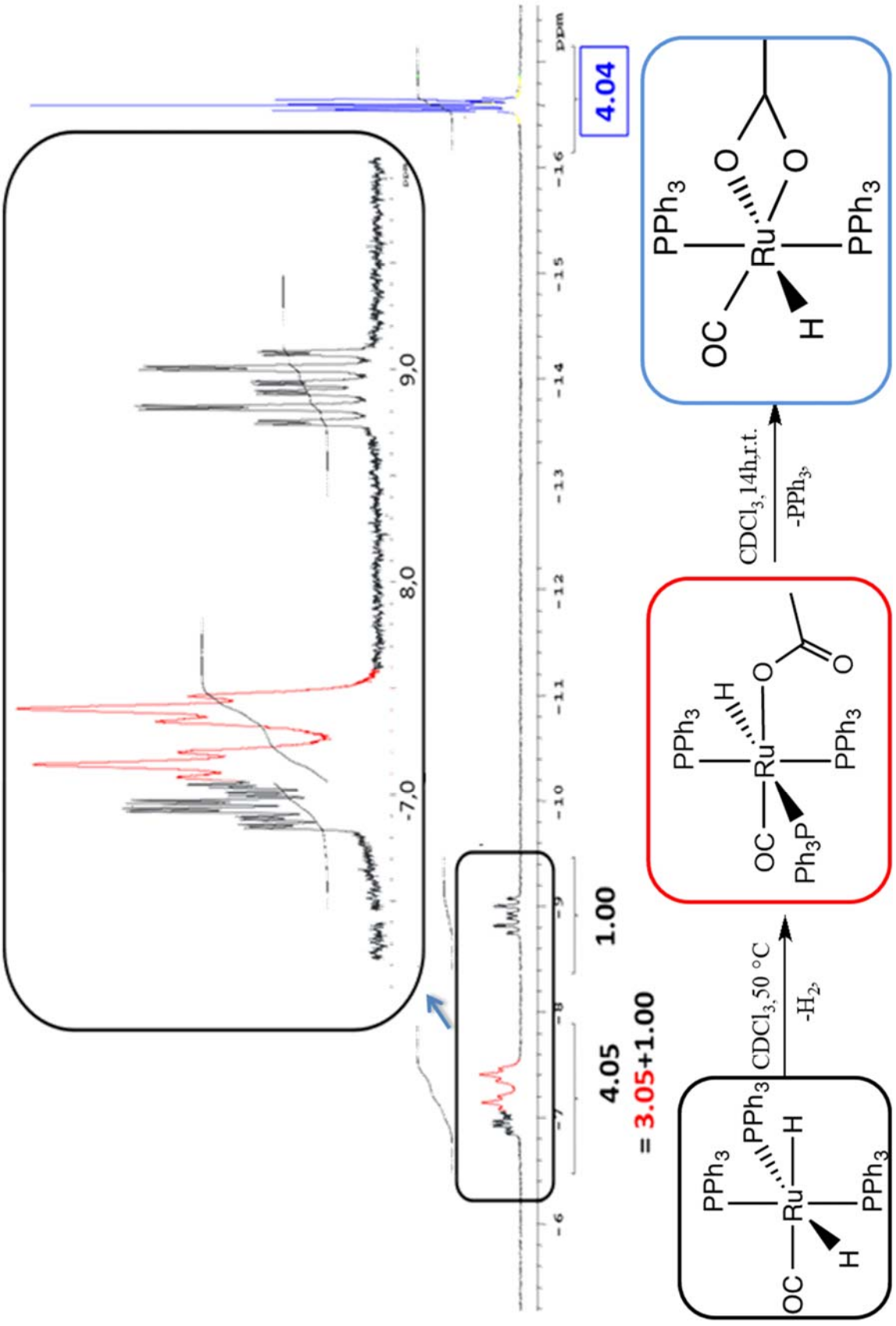

Figure S13. ^{1}H-NMR hydride region spectrum of **1**+**5**+**6** in $CDCl_3$

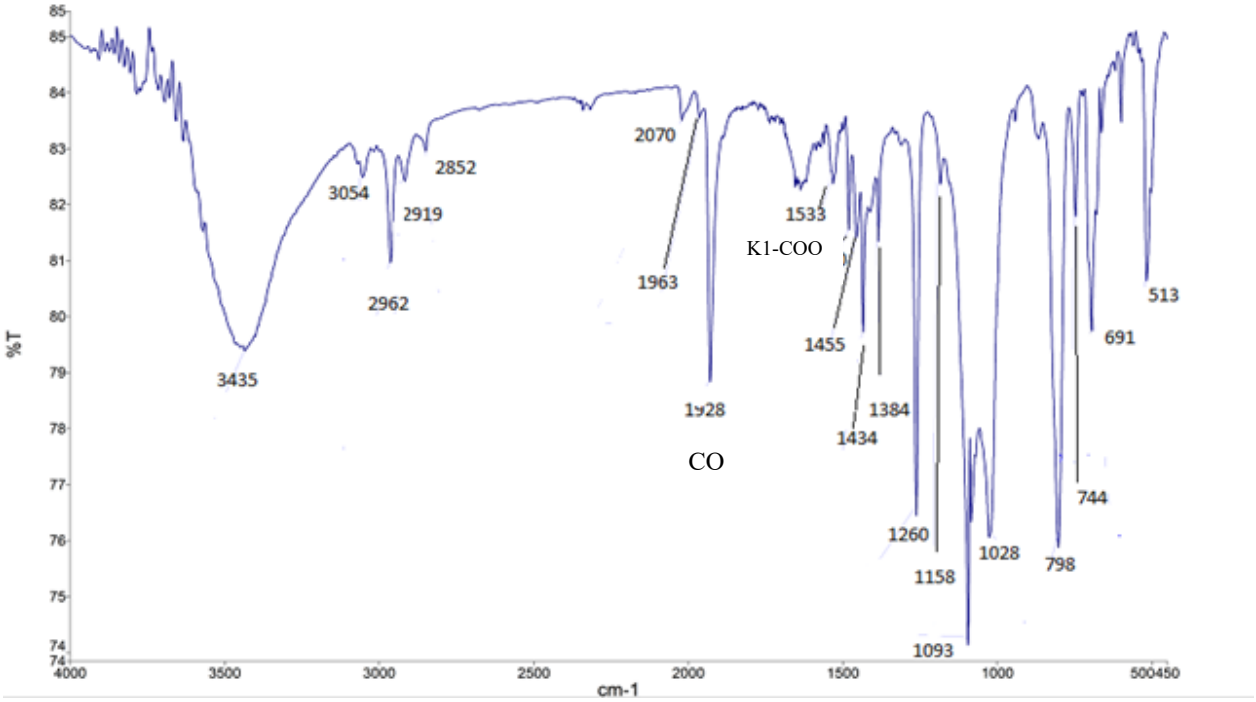

Figure S14. FTIR of compound κ^1(O)Ac-[RuH(CO)(PPh_3)$_3$] **5**

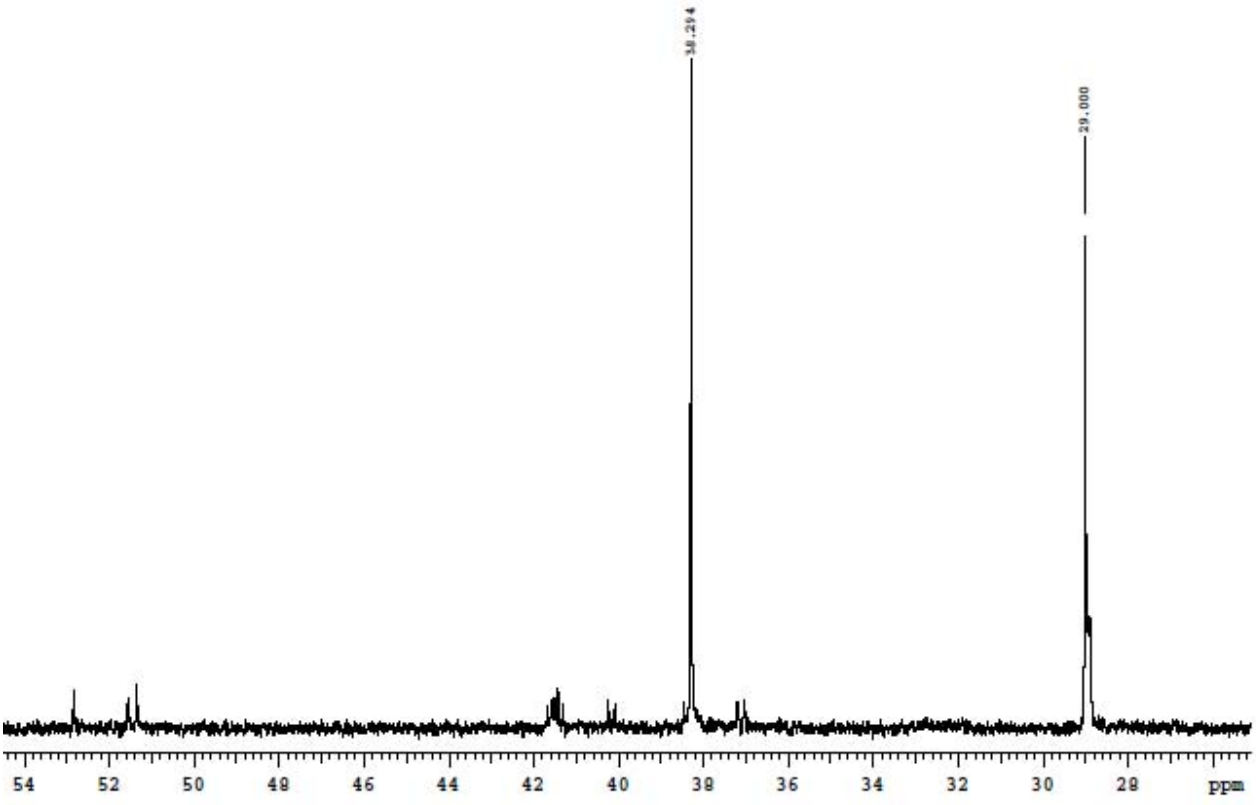

Figure S15a. $^{31}P\{^{1}H\}$-NMR spectrum of **6** species.

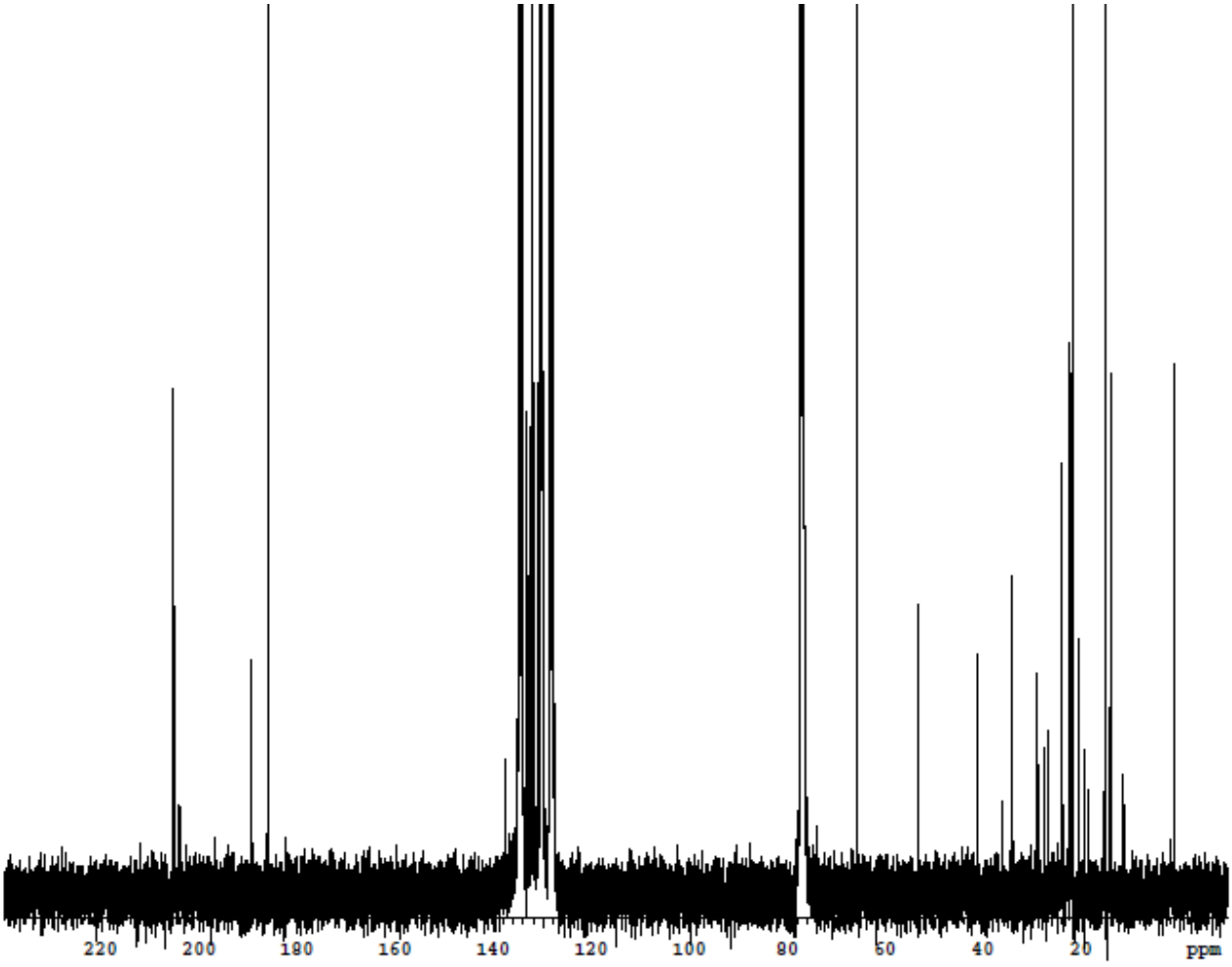

Figure S15b. $^{13}C\{^{1}H\}$-NMR spectrum of **6** species.

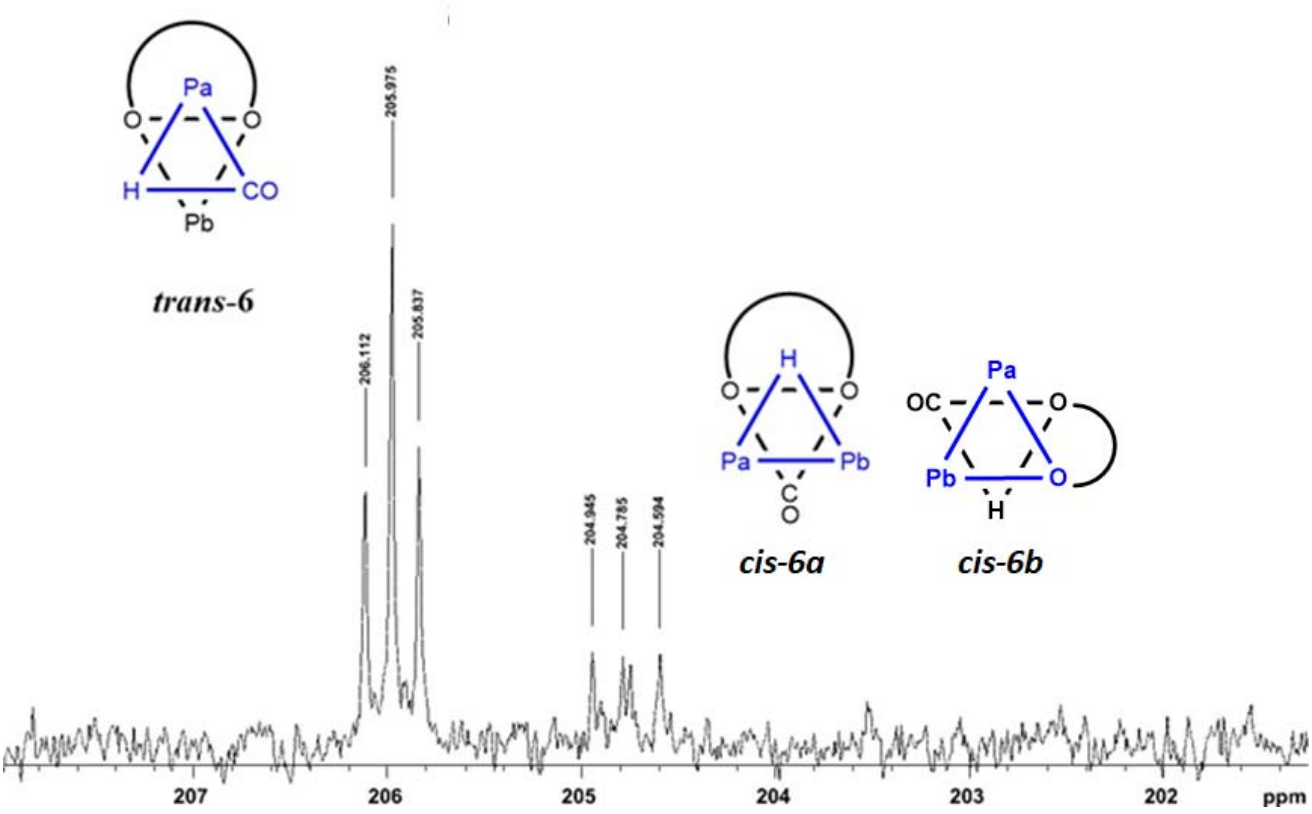

Figure S15c. $^{13}C\{^{1}H\}$-NMR spectrum of **6** species.

Figure S16. FT-IR (KBr) κ^1(O)Ac-, κ^2(O,O)Ac-[Ru(CO)(PPh_3)$_2$], **7**

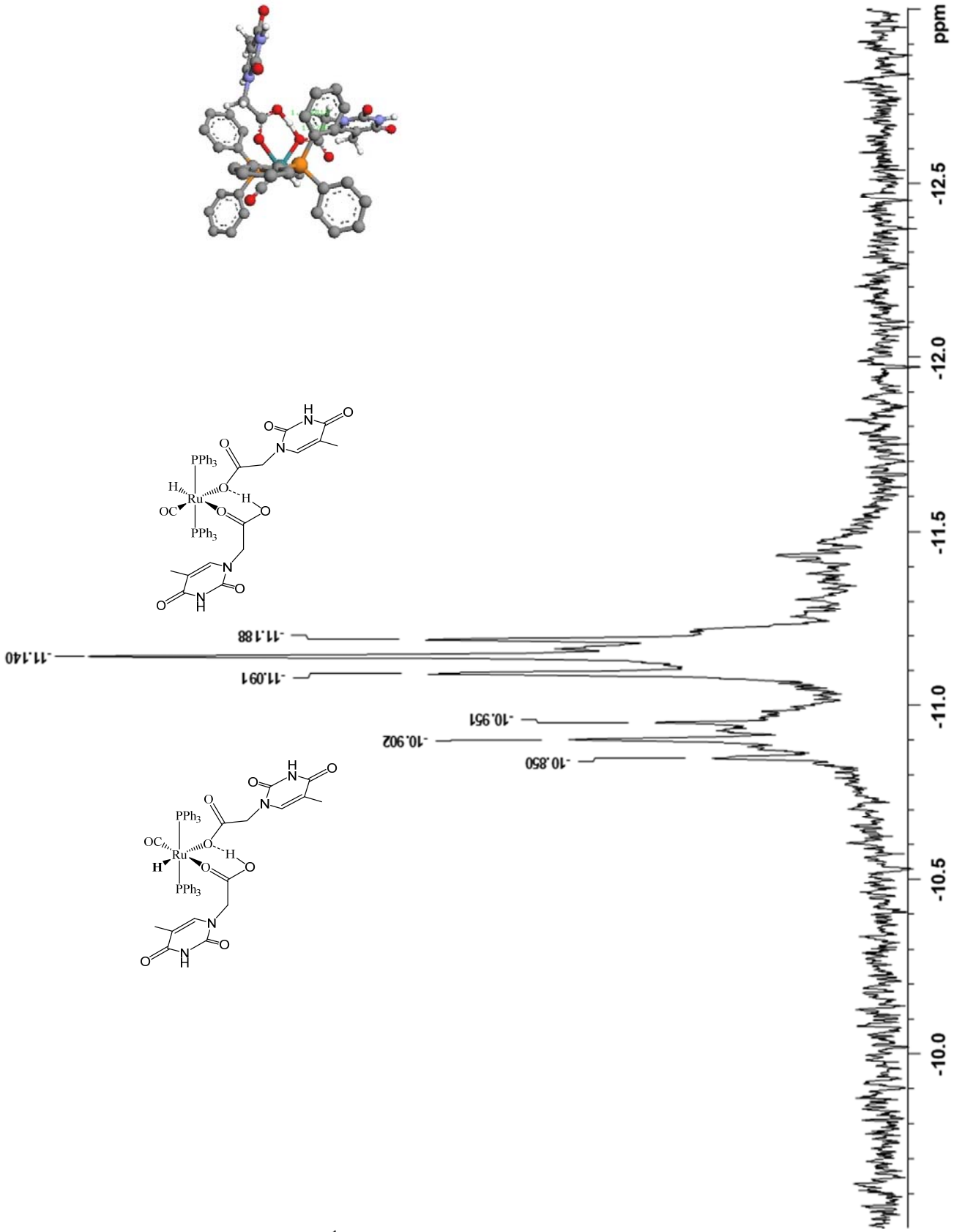

Figure S18a. Portion of hydride in ^{1}H-NMR spectrum in $CDCl_3$ of plausible intermediates of the type $\kappa^1(O),\kappa^2(O)$-[$THCH_2C(O)O\cdots H\cdots OC(O)CH_2TH$][$Ru(CO)H(PPh_3)_2$], **A** analogous to **B** intermediate

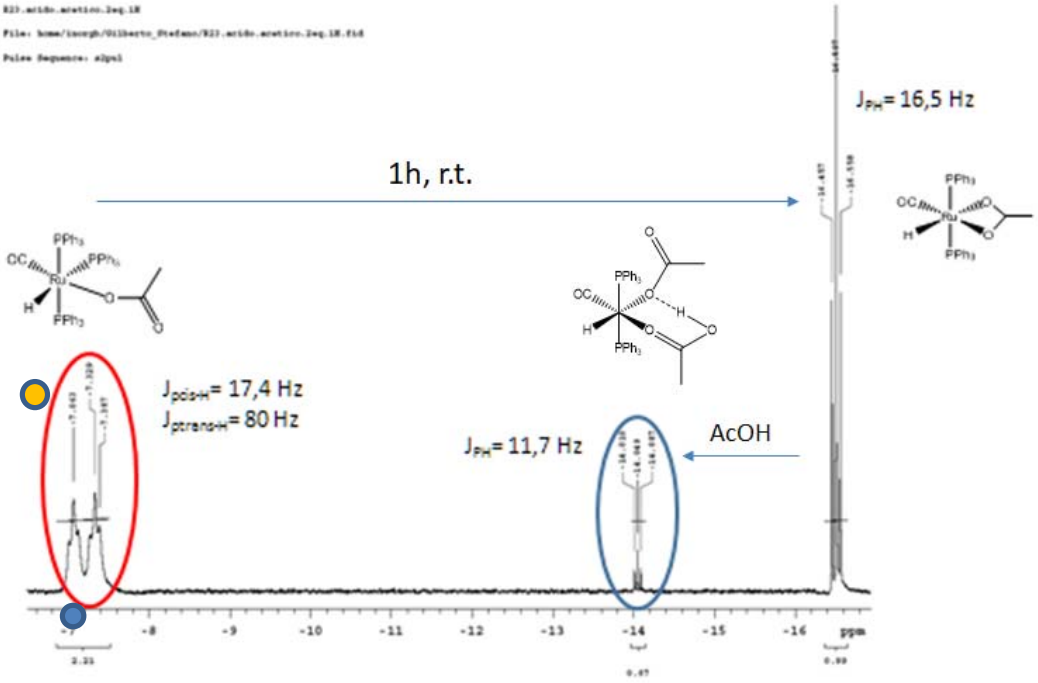

Figure S18b. Portion of hydride in ^{1}H-NMR spectrum in $CDCl_3$ of plausible intermediates of the type $\kappa^1(O),\kappa^2(O)$-[MeC(O)O···H···OC(O)Me][Ru(CO)H(PPh_3)$_2$] **B**.

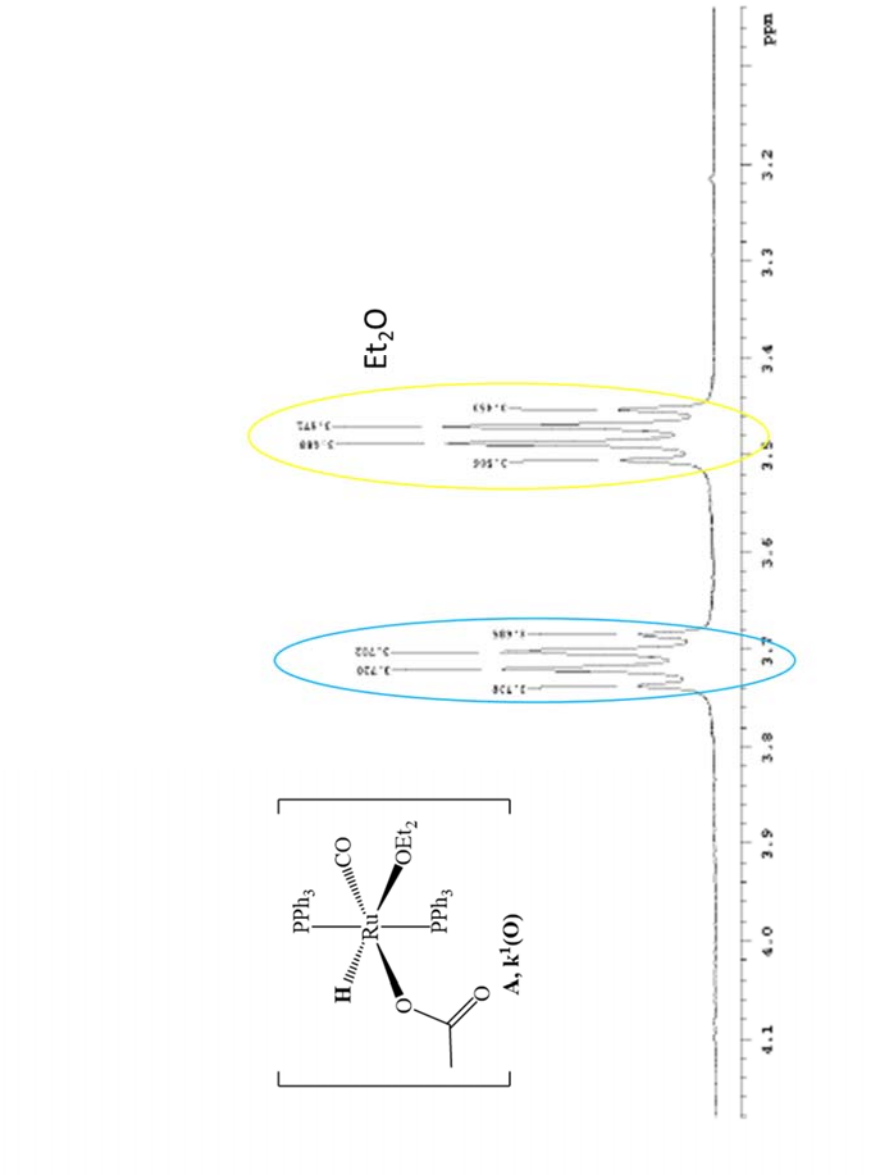

Figure S18c. ^{1}H-NMR portion of the spectrum of **A** in $CDCl_3$ displaying the CH_2 moiety of the Et_2O solvent, remarkably shifted upon Ru-coordination

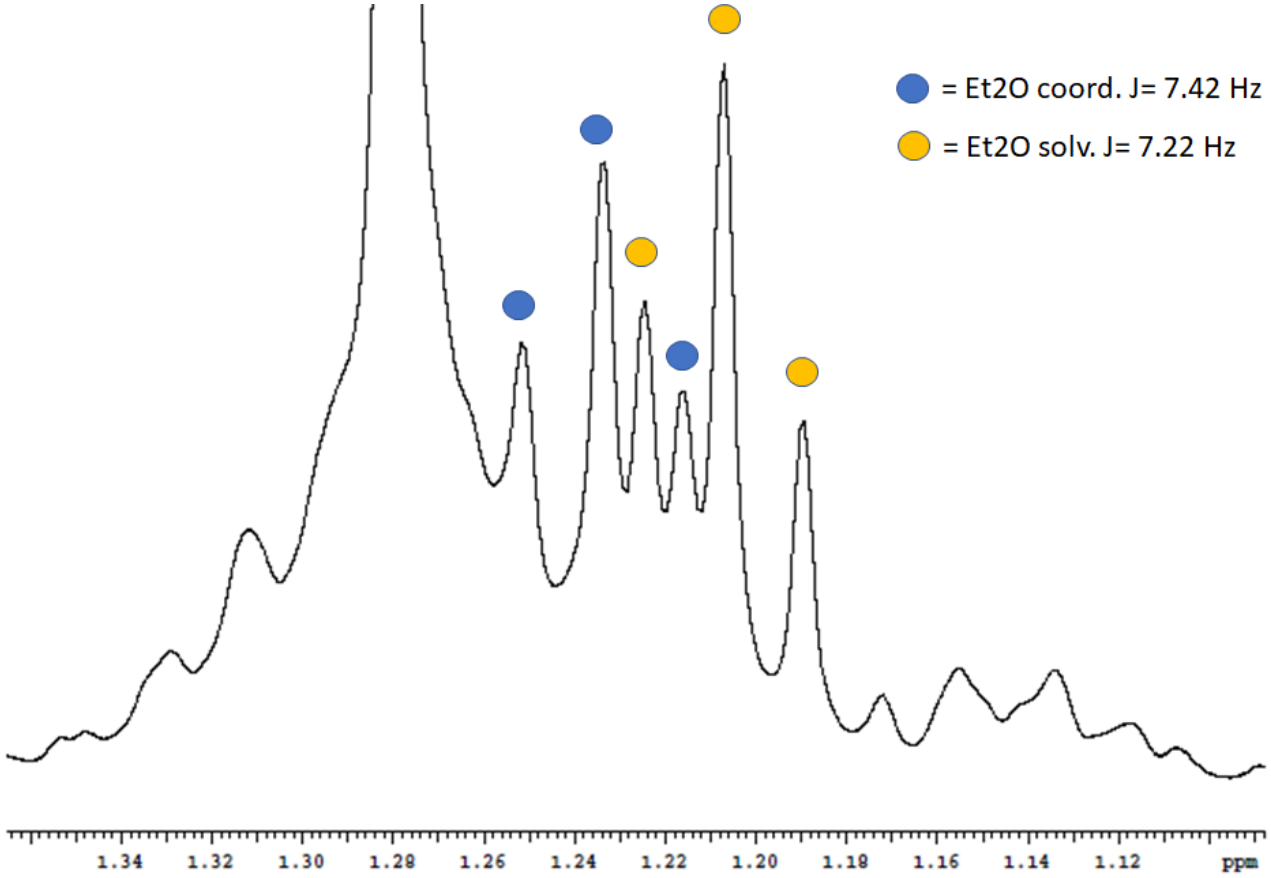

Figure S18d. ^{1}H-NMR portion of the spectrum of **A** in $CDCl_3$ displaying the CH_3 moiety of the Et_2O solvent, shifted upon Ru-coordination